

# Contrastive Deep Learning Reveals Age Biomarkers in Histopathological Skin Biopsies

Kaustubh Chakradeo<sup>1,+,\*</sup>, Pernille Nielsen<sup>2,+</sup>, Lise Mette Rahbek Gjerdrum<sup>3,6</sup>, Gry Sahl Hansen<sup>3</sup>, David A Duchêne<sup>1</sup>, Laust H Mortensen<sup>4,1</sup>, Majken K Jensen<sup>1,7</sup>, and Samir Bhatt<sup>1,5,7,\*</sup>

<sup>1</sup>University of Copenhagen, Section of Epidemiology, Department of Public Health, Copenhagen, 1353, Denmark

<sup>2</sup>Technical University of Denmark, Department of Applied Mathematics and Computer Science, Kongens Lyngby, 2800, Denmark

<sup>3</sup>Department of Pathology, Copenhagen University Hospital- Zealand University Hospital, Roskilde, Denmark

<sup>4</sup>Danmarks Statistik

<sup>5</sup>Imperial College London

<sup>6</sup>Department of Clinical Medicine, University of Copenhagen, Copenhagen, Denmark

\*chakradeo@sund.ku.dk, samir.bhatt@sund.ku.dk

+these authors contributed equally to this work

7these authors contributed equally to this work

## ABSTRACT

As global life expectancy rises, so does the burden of chronic diseases, yet individuals exhibit considerable variability in the rate at which they age. Identifying biomarkers that distinguish fast from slow ageing is crucial for understanding the biology of ageing, enabling early disease detection, and improving prevention strategies. Using contrastive deep learning, we show that skin biopsy images alone are sufficient to determine an individual's age. We then use visual features in histopathology slides of skin biopsies to construct a novel biomarker of ageing. By linking with comprehensive health registers in Denmark, we demonstrate that visual features in histopathology slides of skin biopsies predict mortality and the prevalence of chronic age-related diseases. Our work highlights how routinely collected health data can provide additional value when used together with deep learning, by creating a new biomarker for ageing which can be actively used to determine mortality over time.

## Introduction

### Background- Ageing

The global population is ageing fast due to fast declining mortality rates. As demographic pyramids shift to an older population, it is essential to understand what drives the enormous heterogeneity in how people age. From a public health view this is the matter of why, for a particular age, some individuals experience more senescence and frailty, while others remain comparatively healthy<sup>1</sup>. The observation that physiological differences underpin this variation has led to a distinction between chronological and the so-called biological age.

Various forms of epigenetic alterations like loss of histones (proteins around which DNA can wind for gene regulation), telomere length, as well as histone modification, and DNA methylation (methyl groups attached to DNA molecules) have been suggested to be biomarkers of cellular ageing. Existing methods for defining biological age typically rely on linear regression functions of hallmarks of ageing including sets of biomarkers like e.g., telomere length, DNA methylation, mitochondrial dysfunction or various "-omics")<sup>2-5</sup>; however, no clock captures all the hallmarks of ageing. It is also difficult to decide which combination of biomarkers should be used to capture ageing clocks<sup>6-12</sup>. The biological age of an individual is, therefore, the *predicted age* estimated by a given model, and the metric that becomes interesting for the individual is reduced to the difference between biological and chronological age as a way to detect accelerated ageing, in other words, biologically ageing faster than the chronological age peers.

The primary question that remains is whether the developed biological age is a better measure of residual age (or "ageing status") as compared to chronological age. Measures of biological age are therefore often evaluated in terms of their ability to predict adverse outcomes such as death or incidence of age-related disease<sup>4,13</sup>. In other words, is biological ageing a better measure for risk of mortality for a given age, over chronological age? One of the ways an estimate of biological age can be determined is by using healthy skin samples: trained human observation alone reveals that the skin cell profile changes with age<sup>14,15</sup>. The relative numbers of endothelial cells, endotheliocytes, keratinocytes, mastocytes and fibroblasts in the biopsy

samples can be a good indicator of the age of the participant<sup>16,17</sup>. This leads naturally to the question - how do the differences between the chronological age and biological age manifest in prediction tasks for diseases and mortality? Age itself can be a driver of diseases, acting as a risk factor for a wide range of diseases like cardiovascular diseases, cancer, neurodegenerative disorders, and diabetes among others. However, ageing itself involves numerous interacting factors like gene expression and mutations; understanding these mechanisms can be a key to reduce the risk of age-related disorders.<sup>18,19</sup>

partridge2010new, kirkwood2011systems

### **How can biological age be utilised for prediction tasks?**

Previous studies developing a metric of biological age tend to test ageing against outcome as a criterion validity. However, as mentioned earlier, ageing itself can be a critical factor in mechanisms of disease. It is therefore critical to establish whether biological age has a connection with the risk of disease and mortality. Here, we focus on the discovery of biomarkers that add predictive value in terms of age-related health outcomes. Importantly, the predictive power of an estimate of biological age is expected to perform better than the predictive power of chronological age and sex alone. Some studies have developed definitions of biological age which correlate almost perfectly with chronological age, therefore explaining no variance in outcome that cannot be explained by age alone. Other studies have developed definitions of biological ages that are based on data that pose a risk to the patient (e.g. X-Ray imaging data<sup>20</sup>) or data which are financially costly and do not lead to predictive power that outperforms readily obtainable physiological measures.

While many definitions of biological age focus on specific biological or physiological processes (telomere length, DNA methylation, -omics, physiological measures, etc.) composite definitions that combine information from several types of processes into a single index tend to perform better<sup>5,21</sup>. The propensity for multidimensional markers to perform better supports the notion that ageing is a complex process that manifests at multiple biological scales across all tissues. Here we explore age-related changes in the skin as a low-risk, low-cost, multifaceted manifestation of the ageing process, encompassing alterations in tissue structure, cellular composition, and molecular dynamics.

### **Deep Learning approaches towards pathobiology, ageing and mortality**

By leveraging contrastive deep learning methods to extract visual features in histopathology slides of skin biopsies, we develop a biomarker of ageing that includes features spanning several physical scales, ranging from nanometres to centimetres. As the body's largest organ, the skin undergoes noticeable changes with advancing age. Biopsies taken for disease detection do not pose a large risk for patients, thus making them a valuable target for investigating the underlying mechanisms of ageing even as they are used for other purposes.

This study utilises the vast collection of tissue biopsies, initially collected for clinical purposes unrelated to research, which are stored in the archives at Danish Pathology departments. These biopsies present a unique opportunity, given their diversity in patient age, sex and the broad spectrum of diseases they were originally intended to investigate. Additionally, the biopsies can be linked to comprehensive Danish health registers, providing a comprehensive follow-up with detailed disease trajectories for the patients from whom biopsies were retrieved. This adds value to the biopsies as a resource for discovering biomarkers of ageing and age-related diseases.

The use of deep learning (DL), particularly convolutional neural networks (CNNs) in histopathology has led to several forms of automated analyses in the field. DL models can identify and classify structures on a tissue level as well as cellular and sub-cellular levels. Because of improvements in digital pathology and acquisition of whole-slide images (WSI), as well as the advances in hardware and computing costs, DL models have allowed for leaps in biomedical data analysis<sup>22</sup>. Along with this, the biggest advances have been possible because of increasingly large open-source datasets, like CAMELYON<sup>23</sup>, which was a large collection of fully annotated WSIs of sentinel lymph nodes of patients with breast cancer. Two other open source cancer-related influential datasets with multiple modalities include the Cancer Genome Atlas (TCGA) and Clinical Proteomic Tumour Analysis Consortium (CPTAC). With these tools at hand, DL approaches are now being used for tumour detection and classification<sup>24-37</sup>, image segmentation<sup>38-48</sup>, cell detection, counting and mitosis<sup>49-54</sup>, and tumour grading<sup>55-57</sup>.

However, these approaches have several challenges related with the nature of WSIs<sup>58</sup>. First, the size of WSIs is generally considerable (up to 100000<sup>2</sup> pixels, which is far greater than the typically 224<sup>2</sup> pixels that CNNs can handle). This challenge has been overcome by either creating smaller patches and performing analysis on these smaller patches consisting of cellular and sub-cellular features<sup>59,60</sup>. Another approach has been to use streaming CNNs for end-to-end learning instead of using patches<sup>61</sup>.

The biggest challenge, hand-in-hand with size, is the lack of manually annotated training samples. There have been only a handful of open-source datasets with manual annotations<sup>54,62,63</sup>, making it difficult to train large CNN models. A promising solution comes with the advent of self-supervised learning models, which learn implicit label representations from unstructured data. Even without extensive manual annotations, there is mounting evidence that DL methods are able to predict diseases using WSIs<sup>64-66</sup>. DL methods are also being leveraged to extract ageing-related biomarkers from various medical imaging modalities like X-rays and Magnetic Resonance Imaging, as well as surveys and bio-banks<sup>67-72</sup>.

Here, we make the most comprehensive test to date of deep learning techniques for extracting age-related information from digitised skin biopsy samples. We then aimed to establish a connection between predicted biological age and mortality. For this purpose, we constructed a skin biopsy cohort consisting of 1787 digitised WSI skin biopsies from age-stratified and sex-specific patients with a wide age range and even distribution of males and females. We linked together these WSI skin biopsy samples with prevalent age related diseases as well as mortality using the Danish Registers. Using deep learning models, we were able to extract ageing-related features from these biopsies, and then use the extracted ageing information to predict the prevalence of various age-related diseases. Additionally, we were able to plot the probability of risk of mortality over a set time period by using the incidence of these diseases and the extracted biological age from the deep learning model. We demonstrate how these measures lead to a clear link between ageing information extracted from biopsies and mortality.

## Results

We developed a novel deep learning-based system to extract sex-specific age-related feature information from digitised skin biopsies. The added predictive value from the visual features is assessed in several analyses, coupling the biopsy data to information of disease and survival. We find that the visual features add predictive value above and beyond age and sex alone (Fig. 1D). We also investigated which visual features constitute the highest predictive power towards age, and discuss how these features relate to known morphological features in the skin tissue ( Fig. 3).

Our system consists of 4 components (Fig. 1): (a) Data Collection, b) Preprocessing and self-supervised pretraining to extract visual information related to age from digitised skin biopsies, c) Prediction of age and d) Downstream tasks using predicted age to check for the usefulness of the visual features extracted from the skin biopsies. In a) we collected digitised biopsy samples of 919 males and 868 females from the Danish National Register of Pathology (DNRP). We followed this cohort over a span of 20 years since the first biopsy, during which death eventuated for 230 males and 118 females. We preprocessed the biopsy in b) by first creating patches from whole slide biopsy images in different scales depending on the resolution of the digitised biopsies, with one scale having a maximum patch size of 1024x1024 pixels and the second scale having a maximum patch size of 4096x4096 pixels. Only the patches containing the biopsy part in the foreground were selected. We downscaled all patches to 224x224 pixels for fit as input separately for the VGG-based self-supervised contrastive deep learning model (CDL). The different scales allow for the model to focus on either tissue information or cellular and sub-cellular information. We ran this CDL twice, once for each scale, and extracted features from the patches in the form of vector embeddings. Using these feature vectors, we used an xGBoost model<sup>73</sup> to predict the age of each participant in c). We first clustered these feature vectors so that patches with similar features belonged to the same cluster. Taking this predicted age, in d) we performed downstream tasks to verify the validity of using predicted age to classify prevalent diseases at the time of biopsy using logistic regression, then using these predicted ages and diseases for predicting survival probabilities using these prevalent diseases over 20 years, using a cox regression model<sup>74</sup>. To find out the utility of using predicted age versus using the actual ages of the participants, we compared the results of d) with using actual age with the same model settings. The biological plausibility of the link of extracted features with age was then checked by visualising the age-related feature information in Fig. 3.

Our analyses show that features extracted from skin biopsies can give a good indication of the age of participants across all ages, for both males and females. This can be verified using 3 different criteria; first, visualising the best-performing features in terms of their mean absolute error (MAE) between the actual ages and the predicted ages (Fig. 3). We find that these features are indicative of biopsy characteristics such as atrophy of the epidermis and damaged collagen. The second criterion we use to verify the predicted ages is by taking them as a proxy for actual age in age-related prediction tasks - a common estimation question in epidemiology. Using MAE as a metric, we find that these predicted ages perform better than using the actual ages for predicting 7 age-related indecent diseases, that is, diseases which participants had at the time of biopsy. Finally, we verify the predictive power of biopsy samples for age by using it instead of actual age to predict the survival probabilities of the participants. Once again, we find that the extracted features perform either on par or outperform using actual ages in predictions of survival. Using these three criteria, we can confirm that features extracted from skin biopsies using deep learning models are explainable, can predict age of participants well, and often perform better for further predictive tasks in comparison to actual ages.

### Features from contrastive deep learning correlate with age

WSIs from biopsies were first converted into smaller patches, as the large size can complicate their use for contrastive deep learning model (CDL) (Fig. 1 b). In order to extract visual features representing different physical scales, we constructed patches of two different scales, 1024x1024 pixels for scale 1 and scale 2 with a maximum size of 4096x4096 pixels. Thus, based on the dimensions of the patches, keeping the resolution constant, patches in scale 1 contained more tissue-level information, while scale 2 contained more cellular and sub-cellular information. Using our CDL model we then extracted visual features from each patch, resulting in many sets of visual features for each biopsy (each WSI). We used this CDL model twice, once for each scale, and thus had two sets of visual features, with 512 features for scale 1 and 128 features for scale 2. For each scale,

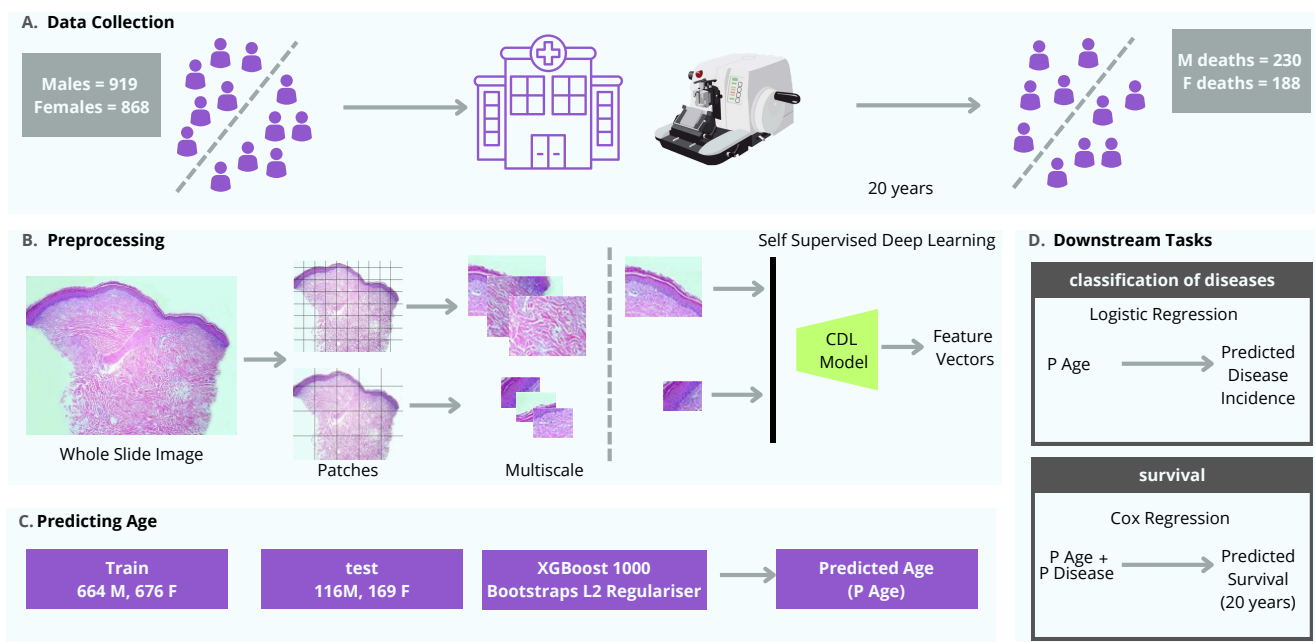


**Figure 1.** Overview of the Workflow

A) Data Collection: The samples are from the Department of Pathology, Zealand University Hospital from the Zealand region in Denmark, consisting of 919 males and 868 females. These samples are digitised, and information relating to their age, sex, medical history and mortality is linked using national registers at Statistics Denmark (DST). B) The whole slide digitised biopsy images are converted to smaller patches of 2 scales, with a maximum size of 1024x1024 for scale 1 and 4096x4096 pixels for scale 2. Patches containing skin information were selected and further downsampled to 224x224 pixels as separate inputs to the contrastive deep learning model (CDL). First, the patches are contrastively augmented (Methods ) into 2 views (V1 and V2). The encoder model is used to transform the output of V1 onto V2, while the weights for V2 are not updated. The views are compared using cosine similarity loss. The predictor model then generates vector embeddings of each image V1, which we call features vectors, or simply, features. C) These features can capture age-related information and thus are used to predict the age of the participant using an xGBoost model with 1000 bootstraps with a ridge regression optimiser. D) The predicted age is used in two downstream tasks to first classify 7 age-related prevalent diseases and compared with using only the actual ages. These prevalent diseases, along with the predicted ages from C are used to calculate the survival probability over 20 years (time since the first biopsy) to validate whether the features extracted from the biopsies from the CDL can be utilised as a proxy for actual ages.

we reduced the amount of patches contributing per patch, by clustering similar patches together using a K-means clustering algorithm and aggregating the features belonging to similar clusters together. Thus, we converted the varying amount of patches for each biopsy to 3 clusters, with their feature sets, over 2 scales. We then also included a third scale for analysis by combining scales 1 and 2, testing if a combination of tissue information and cellular and sub-cellular information can work better than either individually.

The extracted visual features were then used to predict age at the time of biopsy, drawing out any age-related information from the biopsies using an XGBoost model with 1000 bootstraps. We found that the predicted ages, which were based solely on features extracted from the skin biopsies, correlated with the actual ages of the participants. Ages were predicted using different scales, as well as combined scales such as scale 3. For both men and for women, we find that scale 1 (containing cellular and sub-cellular information) performs better for males and females for all ages, even though there are no significant differences in the MAE for individual age categories. A likely reason is the lower frequency count for individuals in sub-categories. Table 1 shows individual MAEs for males and females across age categories, as well as for all categories combined.

As seen in the table, for overall ages, the smallest scale 1 outperforms the bigger scale 2 for both males and females. When using the combined scales, the difference is not as great, but still, scale 1 has the most predictive power. That is, the predictions based on features from the CDL model having more patches of smaller dimensions, rather than fewer patches with larger dimensions produced a higher accuracy. Seemingly, sub-cellular features carry stronger age-related information than tissue-level information. When the model has only tissue-level information with the same resolution, it can miss the smaller sub-cellular structures, which contain important biomarkers to ageing like epidermis atrophy, collagen deterioration,

Age	# Participants	MAE (Scale 1- Smaller)	MAE (Scale 2- Larger)	MAE (Scale 1 and 2 Combined)
<b>Males</b>				
0 – 20	100	1.79 (1.75 - 1.83)	1.80 (1.76 - 1.84)	1.80 (1.76 - 1.84)
21 – 30	100	2.18 (2.13 - 2.22)	2.24 (2.19 - 2.26)	2.14 (2.10 - 2.18)
31 – 40	100	2.21 (2.15 - 2.27)	2.52 (2.44 - 2.60)	2.45 (2.38 - 2.51)
41 – 50	100	2.24 (2.10 - 2.28)	2.75 (2.5 - 3.0)	2.72 (2.55 - 2.80)
51 – 60	199	2.46 (2.42 - 2.50)	2.53 (2.47 - 2.60)	2.52 (2.47 - 2.59)
61 – 70	217	2.39 (2.35 - 2.42)	2.53 (2.45 - 2.60)	2.49 (2.40 - 2.57)
≥ 71	103	4.86 (4.74 - 4.99)	5.85 (5.01 - 6.69)	5.03 (4.97 - 5.09)
All ages	919	2.20 (1.7 - 2.9)	5.63 (4.30 - 8.86)	2.55 (1.93 - 3.17)
<b>Females</b>				
0 – 20	99	2.38 (2.32 - 2.43)	2.44 (2.38 - 2.50)	2.41 (2.35 - 2.47)
21 – 30	99	2.60 (2.55 - 2.65)	3.14 (3.06 - 3.22)	2.65 (2.55 - 2.75)
31 – 40	100	2.3 (2.23 - 2.37)	2.68 (2.60 - 2.75)	2.43 (2.36 - 2.50)
41 – 50	99	2.50 (2.46 - 2.53)	2.58 (2.52 - 2.63)	2.51 (2.46 - 2.54)
51 – 60	246	2.55 (2.49 - 2.61)	2.74 (2.68 - 2.275)	2.72 (2.67 - 2.77)
61 – 70	153	2.65 (2.60 - 2.71)	2.86 (2.76 - 2.95)	2.69 (2.65 - 2.75)
≥ 71	72	5.49 (5.42 - 5.55)	5.9 (5.8 - 6.1)	5.6 (5.49 - 5.72)
All ages	868	7.48 (6.82 - 8.16)	10.56 (10.01 - 11.11 )	8.51 (8.07 - 8.95)

**Table 1.** Mean absolute errors between actual age and predicted age by model

and changes in cellular contours from the dermis.

Henceforth, all plots are made using scale 1. Table 1 is also visualised with Fig. 2. The smaller area that each patch covers from a WSI, that is, the more micro-cellular level information the model gets at the highest resolution, the better become the predictions of age signals. When using bigger patches consisting of tissue-level information, the resolution was lowered, and the same model was not able to extract age-related signals accurately. However, we have only compared two different patch sizes and cannot reject that other physical sizes may add additional predictive power to the extracted information. We also find that as the actual age of participants increases, the accuracy of predictive age decreases. For most young participants between the ages 0 to 20, the predicted ages are quite close to their actual ages, however, for females over the age of 71, the mean absolute error between the actual age and predicted age can differ by up to 5.9 years. We attribute this difference to different lifestyle factors, cardiovascular diseases, oxidative stress,<sup>75–79</sup> causing different levels of ageing in adult humans, while these differences are limited for children. We also see that the model is better at predicting age for males, compared to females, when we see overall age predictions.

Table 1 and Fig. 2 both show that there is a difference in ageing between males and females. The difference between the chronological age and biological age markers increases further as women age, compared to males. This is clear from the mean absolute error values in table 1. This variation in females can primarily be seen in age groups above the age of 50, whereas for men, it remains relatively stable for men between ages 50 and 70. Fig. 2 also captures this variation, as we see that the predicted ages for males between 50-65 remain clumped around the actual ages, while in the case of females, there is a lot more variation away from the regression line.

To biologically validate whether features contain age-related information, we also plot the individual patches which contribute the most towards the age predictions, that is, where the MAE for actual ages vs predicted ages is the lowest. These areas represent the key areas of biopsy samples in terms of patches contributing to age-related information. These attention maps highlight various features of the skin biopsy. These features contributed the most towards accurate age prediction. We see from the image that the model is successfully able to extract age-related information from the biopsy patches. The attention maps focus on a combination of different cellular and sub-cellular level information to make a prediction on age.

The attention maps of the models in Fig. 3<sup>1</sup> highlight various features from the skin biopsy. These features contributed the most towards accurate age prediction. We see from the image that the model is successfully able to extract age-related information from the biopsy patches. The attention maps look at a combination of different cellular and sub-cellular level information to predict age. The thickness of the epidermis layer exhibits atrophy with age<sup>80</sup>, and thus becomes an important feature towards age detection. In the figure, the first row shows patches with normal epidermis and dermis without any signs of atrophy or inflammation, which is young and healthy skin. Epidermal atrophy was one of the most important factors for

<sup>1</sup>Note that for privacy reasons, the patches shown in Fig. 3 are patches which have undergone colour and geometric transformation and may look visually different from the original patches.



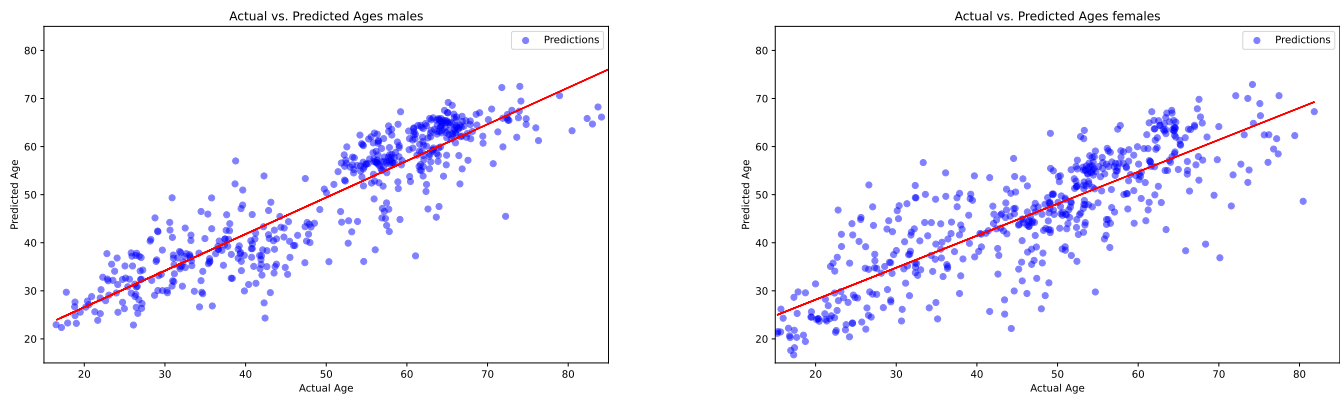


**Figure 2.** Predicting ages using extracted features from the biopsies

predicting age. Similarly, rows 2 to 5 show normal collagen without any degeneration factors, again a sign of young and healthy skin, and an important factor for predicting age. On the other hand, row 6 has a combination of degenerated collagen, and a thin, atrophic epidermis, which were important factors to predict old age. The cellular contours from the dermis of the biopsy also contribute to age information. With age, in the dermal layer, fibroblast cells cannot produce collagen (a protein) as effectively, leading to a weakened skin structure. This is evident in the image, with younger participants having intact collagen, and older participants (50+) having a more degenerated collagen. Because the factor of degeneracy and damage of collagen and epidermis can vary a lot for individual people, it is more difficult to predict older ages, compared to the undamaged skin of younger people. Nevertheless, the amount of damage and degeneration of the epidermis and collagen was an important factor for the model in predicting ages.

Biopsies are not usually performed on normal and healthy skin. Hence, most samples used in this project were resection specimens for nevi or other causes. Despite restricting our samples to biopsies without recorded skin neoplasia, some patches did in fact contain melanocytic nevi. These are benign lesions, however, some can develop into melanoma over time. Since the total number of patients is low, and the amount of patients with nevi are even lower (34), it is not feasible to train a deep learning model to identify nevi in order to censor them. However, they become interesting features towards age for the CDL model, nevertheless. Only in participants aged 50+, did the patches containing nevi become important for predicting age. Patches containing nevi among younger people were not seen as important for age prediction. The patches in the figure, in row 8 all contain nevus and are exclusively in the age range of [55, 85]. There is literature which points to changing patterns of nevi according to age, which can be evidenced by the model decisions based on the figure.

In addition to these common features, there are also features not present in a majority of the participants, which still become important indicators of age for the deep learning model. These are patches containing features like hyperkeratosis, sebaceous glands, pigmented epidermis, and muscle fibres. These individual features are not present very often among participants, nevertheless, they become important indicators of age for the CDL model.

When investigating which features in the WSIs contribute the most to predicting chronological age we found that patches showing damaged or atrophic epidermis, and degenerated collagen appeared among the top contributors for old age, while normal collagen, thicker epidermis appeared amongst the top contributors for a sign of healthy skin, that is, young age. These findings align well with known histo-pathology and verify that the CDL model is in fact able to pick up real morphological and histological features, thereby also providing suggestions for future focus points when investigating skin biopsies in the clinic.

### Validating the quality of age-related signals extracted using contrastive deep learning model

Above, we have seen that age-related signals can be extracted from skin biopsies using CDL. We also saw that the CDL could identify important age-related factors extracted from the biopsies. Now, we validate the quality of this signal. How useful is the age information extracted by the CDL? To verify that, we perform 2 classic epidemiological tasks- prediction of prevalent diseases and survival analysis. This is done by predicting the prevalence of several age-related diseases using only the predicted age and sex of the patients. The information extracted from the biopsies enters the prediction model through the predicted age values. We then compare the results to an equivalent model where actual age at the time of biopsy is used instead of predicted age - representing the case where no information is gained from the biopsies. This experiment was done to see if the signal of age-related obtained from extracting features from biopsies had any significant gains over using the traditional actual ages.

In table 2, we compare the classification accuracy for 7 age-related diseases. We applied a logistic regression model to predict the existence of age related diseases, at the time of biopsy as seen in the Danish Registries. We compared using actual ages to predict prevalent disease, vs using the predicted ages (Fig. 1 c). We also used both the predicted age and actual age to



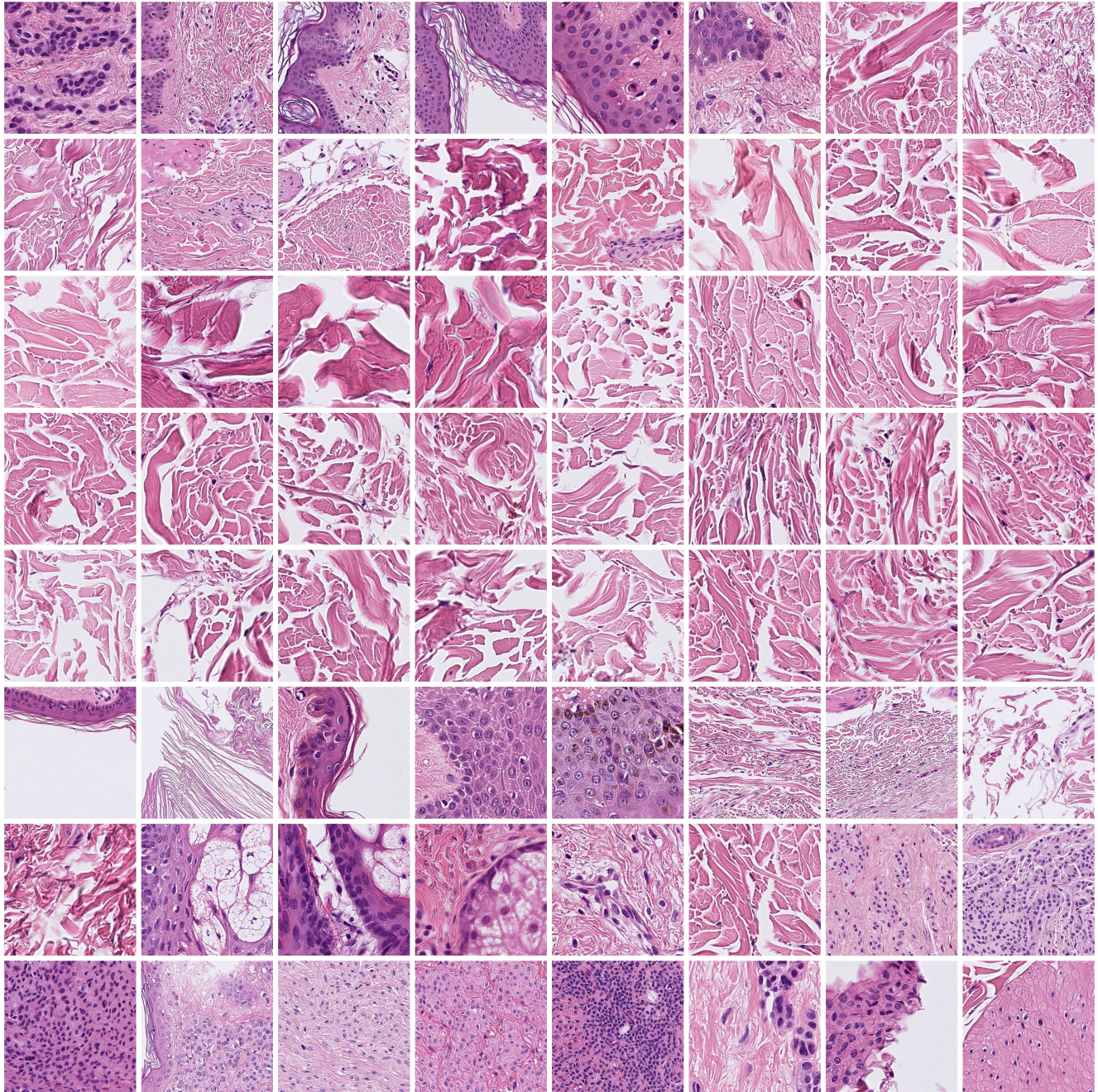


**Figure 3.** Attention maps for predicting age- patches from skin biopsies showing ageing biomarkers



inspect if there are any performance differences from combining these together, as well as seeing if the predicted ages contain any other signal than just age information.

Disease	Accuracy with Actual Age	Accuracy with Predicted Age	Accuracy (Combined)
<b>Males</b>			
Heart Disease	0.949	0.961	0.956
Cancer	0.742	0.804	0.793
Hypertension	0.881	0.945	0.916
COPD	0.946	0.964	0.949
Joint Disease	0.951	0.975	0.973
Osteoarthritis	0.920	0.954	0.947
Osteoporosis	0.957	0.974	0.965
<b>Females</b>			
Heart Disease	0.950	0.972	0.966
Cancer	0.723	0.768	0.744
Hypertension	0.883	0.914	0.899
COPD	0.950	0.962	0.959
Joint Disease	0.941	0.978	0.966
Osteoarthritis	0.932	0.942	0.942
Osteoporosis	0.940	0.941	0.941

**Table 2.** Comparison of Classification Accuracy of Prevalent Diseases with actual ages, predicted ages, and combined age as predictors.

We see that using predicted ages extracted from biopsies gives a slightly better performance than using the actual ages. This provides reassuring evidence of a strong, age-related, signal extracted from skin biopsies using CDL. Another feature is that the performance of using actual age and age-related information factors improves upon the performance of using only actual age. This signifies that not only is the CDL model able to extract important age related information, but also other features which might be useful towards disease prediction. Stated differently, the CDL model captures important residual variation around age. However, to investigate this further, a larger dataset would be needed.

We identify further evidence of age-related information extracted from visual features of skin biopsies. The study population was observed for upto 20 years after the date of biopsy. Again, we compared a model using actual age, verses the same model using predicted age. We plot the hazard ratios of these observed prevalent diseases, as well as the hazard ratios of the predicted prevalent diseases (Fig. 1). We plot these ratios in Fig. 4. On the left, we use only actual or observed ages, as well as prevalent diseases at the time of biopsy. On the right, we use the predicted ages as well as the predicted prevalent diseases from the previous steps. We see no significant difference in the hazard ratios, whether using predicted ages and diseases or using actual ages and diseases. However, some of these predicted diseases (cancer, heart disease) can be seen as significantly associated with death.



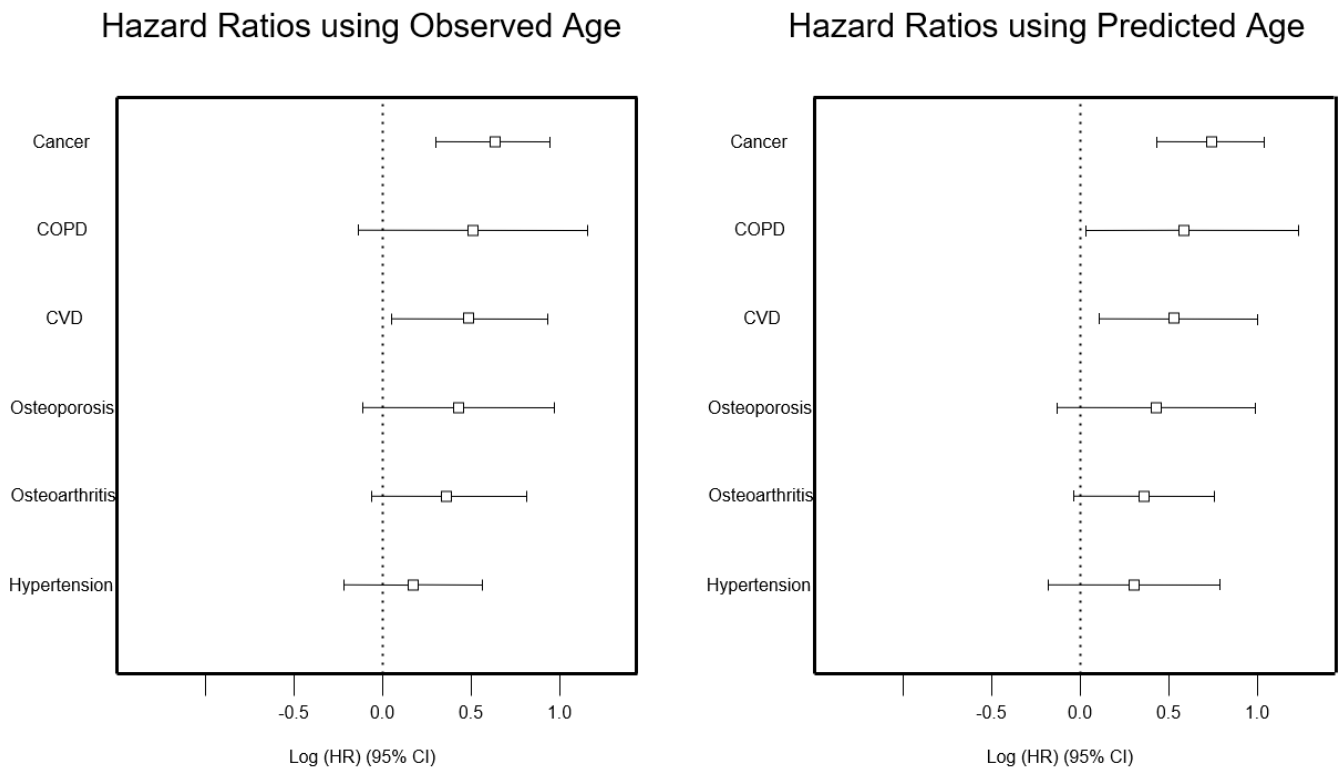


**Figure 4.** Hazard ratios comparison. Left- Using observed or actual age, and actual prevalent diseases at the time of biopsy. Right- Using predicted age and predicted diseases from the CDL extracted features.

We have more evidence that the CDL model can indeed extract age-related information from skin biopsies. This ageing information can then be used for classic epidemiological problems like survival analysis and can be comparable as using their actual ages. We see further evidence that the age-signal that the CDL model extracts from the biopsies can also be used to predict prevalent age-related diseases, and these predictions can be used further for analysing the risk of death. In other words, just extracting information from skin biopsies can be useful even as proxies for diseases and thus measuring the risk of death.

Contrary to the expectation that deep learning models are predictive black boxes, we are able to show the specific features of each biopsy which contribute the most to a decision taken by the model. Fig. 3 lends biological plausibility to the model behaviour and reassurance that salient features are indeed being learned. We see that the factors which are important for the model to predict age, are also reflected by the actual biology of participants. Not only is the model able to extract age-related signals from the biopsies, but it is also able to perform comparatively by using actual ages on multiple epidemiological tasks. Along with age signals, the model is also able to identify features which can contribute to lifestyle and age-related diseases. These factors are also helpful in plotting the survival probabilities of participants over time.

## Discussion

Using Contrastive Deep Learning we have shown that it is possible to extract age-related information from skin tissues from a population spanning a wide age range ([7,94]). After condensing the data from tissue into a predicted age, we have shown that the extracted signal correlates strongly with chronological age, and that predicted age is additionally a high-performance predictor of prevalent age-related disease and mortality hazard. These age-signals also have high performance in classification tasks and survival analysis, comparable to using classical chronological age. Our results provide evidence that easily accessible data from skin tissue have substantial value for capturing the dynamics of human ageing and predicting mortality.

Beyond predicting chronological age alone, detailed registry data allowed us to examine whether the deviation between predicted and chronological ages comprised additional predictive power about disease risk. Indeed, extracted features improved the classification of age-related diseases by up to 4%. These findings provide evidence that not only is it possible to extract age-related information from the skin biopsies, but this approach provides additional predictive power related to the dynamics of human ageing and mortality risk. Our methods, together with similar alternatives, are likely to cast new light on the concept of biological age and on its impact as a tool in clinical and public health settings. However, it has to be said, that biopsies are not performed on normal and healthy skin, but only on participants with some history of skin-related illnesses, usually nevi. All

participants in this study had biopsies performed as part of a routine diagnostic process. This means that the participants, even when we restrict to samples without pathological findings, are likely at higher risk of disease than the background population from which they are sampled. However, the difference is likely most pronounced for the diseases that are diagnosed using skin pathology. It is unlikely that major differences exist in, e.g. mortality. In addition, the findings reported in this paper are within-sample as all participants and included conditional on having a skin sample taken for pathological evaluation.

The use of contrastive learning pretraining is a critical step that facilitates our age-related predictions. Deep learning tasks generally require heavy computation that is rarely available in clinical settings. Our setup bypasses computational requirements and greatly reduces the demands for prediction. Instead of training directly on prediction tasks, the contrastive learning model needs to be trained only once. Once vector embeddings are generated, these can be used in the prediction tasks, and this can be done with simpler regression models that do not require additional GPU computing. Moreover, with a single instance of the contrastive pretraining step, multiple downstream tasks can be performed using the same vector embeddings. This is because in the pretraining step, the model is not trained for any particular purpose, but just to capture information presented in each image. Hence, information related to ageing, diseases and mortality can be captured at once. An added benefit is that to follow data privacy protocols the contrastive step can be done in a completely separate environment, without requiring any labels related to the electronic records. Thus, computing procedures can be done without burdening clinical settings whatsoever. Only the downstream tasks, which do not require GPU computing, need to be done in the clinical setting.

The results presented in this paper are extracted from high-resolution visual micro-structures within the skin. We used different patch sizes to test how varying resolution impacts age-related signals. The smaller area that each patch covers from a WSI, that is, when sub-cellular information is at its highest resolution, the better the predictions of age signals. When using bigger patches consisting of tissue-level information, the same model was not able to extract age-related signals accurately. However, we have only compared two different patch sizes and cannot reject that other physical sizes may add additional predictive power to the extracted information. We found that for young participants, the model was able to extract features like undamaged epidermis and normal collagen, which were the most important factors towards age prediction. On the other hand, for older participants, the model was able to extract the most important features like degenerated collagen and damaged epidermis.

Even when using predicted age extracted from the biopsies, it was found that women had a higher survival probability than males, consistent with established literature<sup>81–86</sup>. The observed ages of males were also closer to the predicted ages in our set, and this could be a feature of the sample used. Alternatively, this might be attributed to diversity in ageing in women versus men. The variance in predicting female age can be attributed to factors like menopause, pregnancy, oestrogen exposure, and other hormonal changes<sup>87,88</sup> - yet not all participants in our study would have experienced all these factors, and those that did would have variance in how they experienced these. Additional demographic information regarding pregnancy and number of offspring among other variables are like to provide further investigation in future work.

Overall, our work places new value on skin biopsy as a strong predictor of age when analysed using our deep learning model. The visual features produced can further be used for high-performance survival prediction. We find that using age information extracted from biopsies to be a better predictor as compared to chronological age from the health registries. The age signals captured by the model suggest that other age predictors, such as the DNA methylation clock, could also be incorporated and provide additional insights into the age-related information from skin biopsies. Further, the pretraining contrastive deep learning step is highly flexible and can be readily scaled to other desired resolutions. We emphasise that training on a large sample size of digitised skin biopsies allows for a vast range of downstream tasks. With more power in the dataset, additional investigations can be done on the link between skin-related diseases and ageing biomarkers. The weights of the pretrained model can also be used to perform downstream tasks like skin lesion detection and find more biomarkers for certain diseases. The biopsy data can also be linked with other omics data like proteomics so that the same contrastive learning model weights are likely useful predictors of protein regulation. In conclusion, contrastive deep learning applied to skin histopathology images is a powerful tool with broad health applications, in a multitude of downstream prediction and detection tasks, under a single heavy computation training step.

## Methods

### Study Overview

Skin biopsies from 1787 individuals (stratified by age and sex, see Table 1) were retrieved from the archives at the Department of Pathology, Zealand University Hospital and digital images were produced for analysis using computer vision (CV)<sup>89</sup>. There were 919 males and 868 females with skin biopsies. The mean observed age (standard deviation) at the time of biopsy of the population was 48.21 (18.14), 47.25 (18.59) for males and 49.19 (17.63) for females. The period for biopsies was between 2000 and 2015. Since the date of biopsy, there were 227 deaths, with 93 males and 130 females dying between their biopsy and 2020, which was chosen as the end of follow-up period in our study.

We developed a Contrastive Deep Learning (CDL) model to convert the digital images into a set of representative visual features, see Figure 1. In the following we present how we extracted age-related information from the visual features found in the skin biopsies and used these extracted features for downstream tasks like prediction of preexisting diseases and predicting survival probabilities over 20 years.

### Selection and Retrieval of Skin Biopsies

The archives at the Danish Pathology departments store histological tissue samples indefinitely. The histological samples are stored in Formalin Fixed Paraffin Embedded blocks (FFPE-blocks). The FFPE-blocks can be retrieved (e.g., for research purposes) and new thin slices may be cut from the biopsies in order to produce glass slides that can be inspected in a microscope or scanned to save digitised images of the tissue structures.

Since normal tissues are not biopsied, we selected samples from the Danish National Register of Pathology (DNRP) with a naevus, and for which there was excess skin adjacent to the naevus, such that we were able to sample normal skin with no indication of disease.

From DNRP we filtered all skin materials with topology codes for skin from non-sun-exposed areas (SNOMED codes T01000, T02403, T02424, T02430(-A,-B), T02470(-A,-B), T02471(-C,-D), T02480 or T02487), with a morphology code for Naevus (SNOMED codes M87200, M87230, M87400, M87500, M87600, M87611, M87700), with a suiting procedure code (SNOMED codes P11000, P30610, P30611, P30620) and which were requisitioned at the Department of Pathology, Roskilde University within the time period 2000-2015. We excluded materials with cancer (SNOMED codes M8xxxx and M9xxxx with last digit not 0) and materials which had other reasons for being not suitable (SNOMED codes M01111, M09000, M09010, M09011, M09013, M09014, M09020, M09025, M09039, M09070, M09100, M09145, M09150, M09155). After this initial filtering, we selected the materials which had the highest chance of having excess skin adjacent to the naevus, by counting the number of FFPE blocks and number of materials per requisition. We then stratified the samples by sex and (categorical) age and selected a random sample of 100 patients within each stratum, except for the strata with ages >50 years, in which we selected all patients. The stored FFPE blocks from these biopsies were retrieved from the hospital archives and we produced digitised images of the skin tissue structures. Very few biopsies were lost due to technical difficulties and in total we retrieved biopsies from 1787 individual patients. The number of biopsies with each stratum can be seen in Table ??.

SNOMED code	
T01000	Skin
T02403	Skin on flank
T02424	Skin on chest
T02430(-A,-B)	
T02470(-A,-B)	
T02471(-C,-D)	
T02480	
T02487	

**Table 3.** SNOMED codes for non-sun-exposed skin areas

### Image Statistics and preprocessing

A single biopsy is evaluated using a technique called super-resolution microscopy. Digital pathology is the process of evaluating digitised histopathology slides on a computer, rather than on bright-field and immunofluorescent light microscopy (LM)<sup>90</sup>.

In this work, we evaluate these skin biopsies using the help of deep learning techniques. A digitised biopsy, called a whole slide image (WSI) can be 50 Mb to over 6 GB in storage size<sup>91</sup>, or about 80000<sup>2</sup> pixels. The digitised biopsy slides obtained from Statistics Denmark were scanned using the Hamamatsu Scanner (model C13220) and stored in a NanoZoomer Digital Pathology Image (ndpi) format. They were acquired from the Zealand University Hospital, Roskilde. The WSI scans obtained were of two resolutions, 2140 and 4280 pixels per inch (ppi).

For deep learning (DL) models for vision, the average input size is 224x224 pixels, which is far smaller than the average WSI size. We therefore divided our WSI scans into smaller patches with some overlap of 50 pixels between neighbouring patches in order to extract features from each patch instead of the entire image at once. The overlap was used to prevent missing information around patch edges. For the different resolutions, we used different patch sizes. For the WSIs with resolution 2140, each patch had dimensions half that of WSIs with resolution 4280. We created two sets of patches from these WSI slides, first, with a patch size of 512x512 and 1024x1024 pixels, and the second set of patch sizes 2048x2048 and 4096x4096 pixels. The larger patches had a decreased resolution in order to extract features from a larger physical scale. Overall, we extracted features from patches of sizes 512<sup>2</sup> pixels (2.3mm<sup>2</sup>) to 4096<sup>2</sup> pixels (9.57mm<sup>2</sup>). We used equation 1 to determine these sizes.



$$Widthincm = Widthinpixels / Resolutionofimage(pixels/cm) \quad (1)$$

After patching was completed, we applied a selection criteria for choosing patches. A WSI slide also contains the white and grey background of the microscopic slide which was scanned. We removed the patches containing only this background and kept all patches showing the biopsy. This was done using colour thresholding, where the distinct H&E stain can be distinguished from the white or grey background of the microscopic slide.

Before training, all patches from set 1 (512x512 and 1024x1024 pixels) and from set 2 (2048x2048 and 4096x2096 pixels) were further reduced to 224x224 pixels to fit as input into a convolutional neural network (CNN).

### Contrastive Deep Learning (CDL) model for extracting visual features from digitised WSIs of skin biopsies

Contrastive Deep Learning (CDL) is a type of self-supervised deep learning technique for vision tasks. We train a model to align the representations of augmented views of the same image (positive pairs) while diverging the representations of different images (negative pairs). In other words, the model is trained to put similar images together, so as to learn a better representation of the images without labels. The CDL contains two models, an encoder network and a predictor network. We create only positive pairs. These pairs are generated using augmentations. A colour augmentation can be obtained by changing the values of contrast, intensity, saturation and hue of the images, while geometric augmentations can be achieved by horizontal and vertical flipping and rotating the images.

Let us consider a patch from the WSI, called  $V$ . We created two contrasting augmentations to generate two augmented views of  $V$ , called  $v1$  and  $v2$ . Compared to established contrastive methods which perform random augmentations, contrastive augmentations make learning harder for the model during training, thus making the model more robust. Thus, for view  $v1$ , colour augmentations were made using a positive delta, and geometric augmentations were made by only flipping vertically and rotating clockwise. For view  $v2$ , colour augmentations were made using a negative delta, and geometric augmentations were made by only flipping horizontally and rotating anti-clockwise. All augmentations were applied with a probability of 0.75. All augmentations were generated dynamically without generating them in advance. Each patch  $V$  is augmented right before being fed into the neural network for each epoch for training. A full list of augmentations can be seen in table 4.

**Table 4.** Contrasting Augmentations to generate both views,  $v1$  and  $v2$ , of the patch  $V$ . Some augmentations like adjusting brightness, and random crops were applied to both views, while all other augmentations were applied in a contrastive fashion for the different views. Note that all augmentations were applied with a probability of 0.75.

$v1$	$v2$	Augmentation Type	Probability distribution	Scale
Both views				
✓	✓	Random Crop	Uniform	(224 px, 224 px)
✓	✓	Adjust brightness	Uniform	$\pm 0.75$ ( $\Delta 0.75$ )
View 1 only				
✓	×	Random rotation	Uniform	$\pm 90^\circ$
✓	×	Random vertical flip	Uniform	
✓	×	Adjust contrast	Uniform	$\pm 1.9$
✓	×	Adjust saturation	Uniform	$\pm 1.1$
✓	×	Adjust hue	Uniform	$\pm 0.01$
View 2 only				
×	✓	Random rotation	Uniform	$\pm 180^\circ$
×	✓	Random horizontal flip	Uniform	
×	✓	Adjust contrast	Uniform	$\pm 2.5$
×	✓	Adjust saturation	Uniform	$\pm 0.75$
×	✓	Adjust hue	Uniform	$\pm -0.01$

### Loss function

The CDL method is a self-supervised pretraining step before prediction models. It works by maximising the similarity between the different augmented views ( $v1$  and  $v2$ ) for the same biopsy patch. This similarity measure is trained using a cosine similarity loss function, explained in

$$-\cos \theta = -\frac{A \cdot B}{\|A\| \cdot \|B\|} \quad (2)$$

where  $A$  and  $B$  are the two representation vectors (here  $v_1$  and  $v_2$ ).  $\|\cdot\|$  is the  $\ell_2$  normalisation. Cosine similarity ranges between  $[-1, 1]$ , where  $-1$  represents opposite vectors,  $0$  represents orthogonal vectors, and  $1$  means they are the same vector.

We use only positive pair (augmented views of the same image) representations here because the batch size is smaller than the number of sizes. Hence, during a batch, there would be no negative pairs (augmented views from different images or classes), reducing the probability of forming negative pairs from patches in the same slide. Thus, with this loss, the model is encouraged to learn representations that bring positive pairs closer, while pushing away negative pairs.

### Encoder Architecture

The two augmented views,  $v_1$  and  $v_2$  are passed through a VGG-based CNN architecture. The input to this model was a  $224 \times 224 \times 3$  patch of the biopsy. This was propagated through ReLU-activated convolutional blocks of 2, 2, and 3 layers. The resulting 512 dimensional output was compressed using global average pooling before passing through two  $\ell_2$ -regularised and ReLU-activated fully connected layers. Using the loss function given by 2, both  $v_1$  and  $v_2$  were passed to the encoder model. The weights during training were updated for  $v_1$ , while a stop gradient (stop-grad) method was applied to  $v_2$ , that is, the weights from  $v_2$  are not updated. In other words, the stop-gradient method acted to create implicit negative pairs.

### Predictor Architecture

A 3-layer multilayer perceptron (MLP) was attached to the encoder model. MLP was used to transform the output of  $v_1$  to that of  $v_2$ . Since the weights of  $v_2$  were not updated, the MLP received no gradients from the output of  $v_2$  but receives the gradients from the output of  $v_1$ . Thus, the predictor transformed the output of  $v_1$  and matched it to  $v_2$ . The predictor architecture was a simple architecture consisting of two fully connected layers connected with a batch normalised hidden layer. The output of this predictor architecture was a vector embedding representation of each image  $V$ .

The model encoder- predictor architecture is described in figure 5. We call this combined architecture the contrastive deep learning model (CDL).

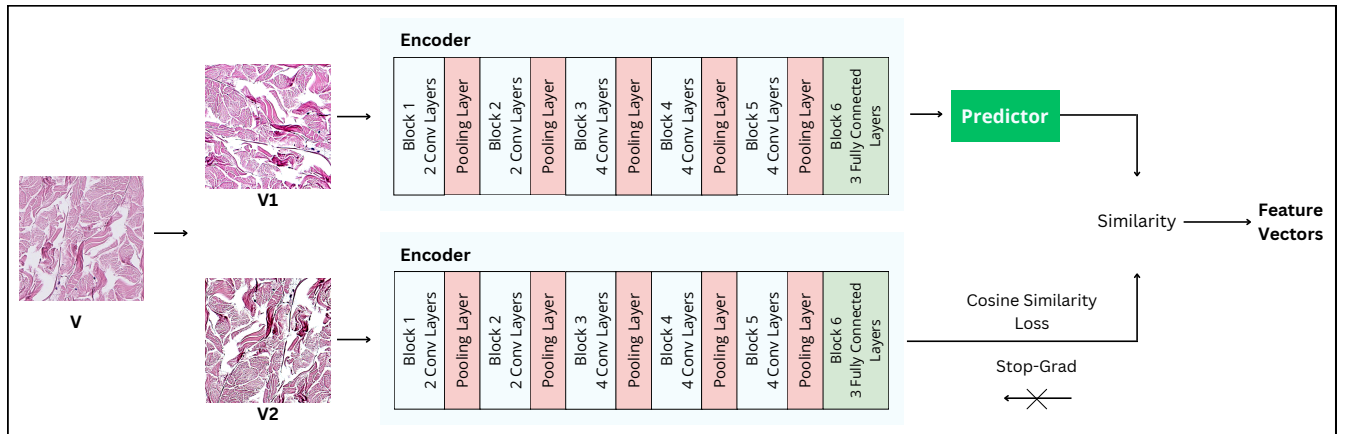


**Figure 5.** Contrastive Learning Method for extracting ageing information from skin biopsies

First, contrastive augmentations are applied on the biopsy patch  $V$  to create views  $v_1$  and  $v_2$ . Both  $v_1$  and  $v_2$  are passed to the encoder. The weights of  $v_1$  are updated, while on  $v_2$ , a stop-grad is applied to prevent weight updation. Using the predictor MLP, the view of  $v_1$  is transformed into the view  $v_2$  using cosine similarity loss. The output of this model is the feature vector embeddings extracted from the biopsies. Thus, after training the CDL model, the representation of biopsy patch  $V$  is transformed from an image to feature vectors.

### Training

This CDL model was trained for 100 epochs, and the biopsy image patches were transformed into vector embeddings from the deep-learning model. This was represented by 1024 different features for each image; the features combined together described the image. After the pretraining contrastive step, each biopsy image patch was described by 1024 features. Pretraining was done on an NVIDIA A6000 GPU.

Disease Group	ICD-10 Code
Heart Disease	I20, I21, I22, I23, I24, I25, I50, I11, I13
Hypertension	I10, I11, I12, I13, I15
Joint Disease	M060, M068, M070, M071, M100, M109
Osteoporosis	M80, M81, M82
Osteoarthritis	M15, M16, M17, M18, M19
COPD	J40, J41, J42, J43, J44, J47, J96
Cancer	Codes below C43.0 and above C45.0
Atopic Dermatitis	L20
Psoriasis	L40
Acne	L70
Rosacea	L71

**Table 5.** ICD-10 codes for disease selection criteria

### Linking CDL output to Demographic Variables from Danish Registries

Each skin biopsy, or WSI has been linked to a participant with a unique personal identification number in the Danish Registries. Using this ID, we linked each biopsy to the date of biopsy, observed age at the time of biopsy, and sex of the participant. Additionally, we also linked death (whether died, or alive, as of 31 December 2020), date of death for participants who had died, and the time from biopsy to end of follow-up (whether death or reaching the mentioned date alive). We also linked if the participant at the time of biopsy had common age-related diseases like heart disease, Chronic Obstructive Pulmonary Disease (COPD), cancer (excluding skin cancer), osteoporosis, osteoarthritis, back pain, joint disease and hypertension. The International Classification of Diseases, Tenth Revision (ICD-10) codes selected are given by table 5.

Some skin diseases like atopic dermatitis, psoriasis, acne, and rosacea were also considered, to evaluate if the model was also able to extract information related to these diseases. The ICD-10 codes for these diseases are also present in table 5.

However, because of the low power of these disease occurrences in the dataset ( $< 100$  in total for all skin diseases combined), these codes were not ultimately used in predictive models analysis. However, a bigger study with a well-represented sample of these diseases could also involve these diseases along with age biomarkers as a prediction metric.

Now, this information was linked to the visual feature set extracted from each patch using the CDL. For each WSI, a KMeans clustering algorithm was used to cluster patch-data into similar groups. Using the elbow method, 3 clusters were created and each patch from a WSI belonging to the same cluster was aggregated. After this, the biopsy images were ready for the prediction tasks.

### Predicting Age from extracted information from biopsies using CDL

The first predictive task was the prediction of age from the learned image features. An XGBoost model was created with 1000 bootstraps, with the pretrained image feature set as predictive variables, with the observed age at the biopsy of the individual as an outcome variable, while adjusting for sex. Predicted age was generated for each category of observed ages for males and females. These predictions were done on three scales, CDL model trained on a scale with a maximum size of  $1024 \times 1024 \text{ pixels}$  (scale 1), CDL model trained on a scale with a maximum size of  $4096 \times 4096 \text{ pixels}$  (scale 2), as well as combining features from scale 1 and scale 2, as explained in table 1 for males as well as females. The accuracy of this model was described using the mean absolute error between observed ages and predicted ages.

### Visualising age related features

For this task, the previous clusters were not used. Instead, for each patch in the biopsy, predictions were made using the model in the previous task, using only scale 1. Then, each biopsy patch was ranked according to the difference in the mean absolute error between the actual age and the predicted age on that patch. The best patches contributing towards the age predictions (least MAE value) were plotted in figure 3.

### Using predicted age to classify age-related diseases

To evaluate whether the age-related information extracted from biopsy samples using CDL was viable, a second prediction task was performed. Each age-related disease linked from the Danish Registries was now set as the outcome variable, while there were two instances of predictor variables- the observed age at the time of biopsy from the Danish Registries, and the predicted age from the previous task. These two instances of predictor variables were compared against each other for each age related disease using a classification task, using a logistic regression model. This model was evaluated using classification accuracy.



## Prediction models for survival analysis

The third task was survival analysis over the next 20 years from the date of biopsy. The long follow-up period was chosen because of the variation in the dates for biopsy (with the earliest being 2000, and the latest being 2015). Individuals were followed until their date of death or end of follow-up, stratified by sex. Again, we did a comparison by using a) the observed age as a predictor variable, and b) the predicted age from CDL as a predictor variable. The existence of comorbidities that each participant had (age-related diseases classified in the previous task) were also added as predictor variables. A Cox regression with  $\ell_2$  norm regulariser model was used to compute the survival probabilities and hazard ratios for each disease. This model was also run as a comparison, first using the actual or observed age and incident disease at the time of biopsy, then using the predicted age as well as the predicted diseases from the previous tasks.

## Acknowledgements

KC acknowledges the grant support from William Demant Fonden (24-3395). KC acknowledges the help of Mignon Hagemeyer for graphical design on the manuscript, and the help of Alexandros Katsiferis for discussions on machine learning based prediction models. MKJ acknowledges the help of Rudi Westendorp who originally envisioned the study.

SB acknowledges support from the Novo Nordisk Foundation via The Novo Nordisk Young Investigator Award (NNF20OC0059309), which also funds KC. SB acknowledges the Danish National Research Foundation (DNRF160) through the chair grant which also supports MPK. SB acknowledges support from The Eric and Wendy Schmidt Fund For Strategic Innovation via the Schmidt Polymath Award (G-22-63345). SB acknowledge funding from the MRC Centre for Global Infectious Disease Analysis (reference MR/X020258/1), funded by the UK Medical Research Council (MRC). This UK funded award is carried out in the frame of the Global Health EDCTP3 Joint Undertaking. SB is funded by the National Institute for Health and Care Research (NIHR) Health Protection Research Unit in Modelling and Health Economics, a partnership between the UK Health Security Agency, Imperial College London and LSHTM (grant code NIHR200908). Disclaimer: ‘The views expressed are those of the author(s) and not necessarily those of the NIHR, UK Health Security Agency or the Department of Health and Social Care.’. DAD acknowledges support from the Novo Nordisk Foundation via the Emerging Data Science Investigator award (NNF23OC0084647). MKJ is funded by the Novo Nordisk Foundation Challenge Programme: Harnessing the Power of Big Data to Address the Societal Challenge of Ageing (NNF17OC0027812), which also funds PYN. LHM acknowledges partial funding from NordForsk (105545), the Novo Nordisk Foundation (NNF17OC0027594 and NNF17OC0027812) and the Villum Foundation (“Nation-Scale Social Networks”).

## Author contributions statement

The study was conceived by PYN and MKJ, while LMRG and GSH designed the study sample and extracted the data. They also were responsible for collecting, selecting and digitising the biopsy samples, and creating the dataset used for the experiment. MKJ, KC and SB conceived and designed the computational study. PYJ was involved in linking the biopsy samples with Danish Registers. KC performed all of the image preprocessing tasks. KC also designed and developed the deep learning modelling, as well as the downstream prediction tasks. KC drafted the initial manuscript and supplementary with input from PYN, MKJ, LMRG and SB. KC prepared the figures. SB was involved in designing the deep learning methodology and downstream tasks. All authors contributed to revising the manuscript.

## References

1. Kojima, G., Liljas, A. E. M. & Iliffe, S. Frailty syndrome: implications and challenges for health care policy. *Risk Manag. Heal. Policy* **12**, 23–30 (2019).
2. López-Otín, C., Blasco, M. A., Partridge, L., Serrano, M. & Kroemer, G. The hallmarks of aging. *Cell* **153**, 1194–1217 (2013).
3. López-Otín, C., Blasco, M. A., Partridge, L., Serrano, M. & Kroemer, G. Hallmarks of aging: An expanding universe. *Cell* **186**, 243–278 (2023).
4. Klemera, P. & Doubal, S. A new approach to the concept and computation of biological age. *Mech. Ageing Dev.* **127**, 240–248, DOI: <https://doi.org/10.1016/j.mad.2005.10.004> (2006).
5. Jylhävä, J., Pedersen, N. L. & Hägg, S. Biological age predictors. *EBioMedicine* **21**, 29–36, DOI: <https://doi.org/10.1016/j.ebiom.2017.03.046> (2017).
6. Sen, P., Shah, P. P., Nativio, R. & Berger, S. L. Epigenetic mechanisms of longevity and aging. *Cell* **166**, 822–839 (2016).
7. Pal, S. & Tyler, J. K. Epigenetics and aging. *Sci. advances* **2**, e1600584 (2016).

8. McCauley, B. S. & Dang, W. Histone methylation and aging: lessons learned from model systems. *Biochimica et Biophys. Acta (BBA)-Gene Regul. Mech.* **1839**, 1454–1462 (2014).
9. Lillycrop, K. A., Hoile, S. P., Grenfell, L. & Burdge, G. C. Dna methylation, ageing and the influence of early life nutrition. *Proc. Nutr. Soc.* **73**, 413–421 (2014).
10. Horvath, S. Dna methylation age of human tissues and cell types. *Genome biology* **14**, 1–20 (2013).
11. Moqri, M. *et al.* Biomarkers of aging for the identification and evaluation of longevity interventions. *Cell* **186**, 3758–3775 (2023).
12. Consortium, A. B. *et al.* Biomarkers of aging. *Sci. China Life Sci.* **66**, 893–1066 (2023).
13. Beltrán-Sánchez, H., Palloni, A., Huangfu, Y. & McEniry, M. C. Modeling biological age and its link with the aging process. *PNAS Nexus* **1**, DOI: [10.1093/pnasnexus/pgac135](https://doi.org/10.1093/pnasnexus/pgac135) (2022). Pgcac135, [https://academic.oup.com/pnasnexus/article-pdf/1/3/pgac135/48942363/pgac135\\_supplemental\\_file.pdf](https://academic.oup.com/pnasnexus/article-pdf/1/3/pgac135/48942363/pgac135_supplemental_file.pdf).
14. Kohl, E., Steinbauer, J., Landthaler, M. & Szeimies, R.-M. Skin ageing. *J. Eur. academy dermatology venereology* **25**, 873–884 (2011).
15. Jenkins, G. Molecular mechanisms of skin ageing. *Mech. ageing development* **123**, 801–810 (2002).
16. Sukhovei, Y., Kostolomova, E., Unger, I., Koptuyug, A. & Kaigorodov, D. Difference between the biologic and chronologic age as an individualized indicator for the skincare intensity selection: skin cell profile and age difference studies. *Biomed. Dermatol.* **3**, 1–16 (2019).
17. Makrantonaki, E. *et al.* Identification of biomarkers of human skin ageing in both genders. wnt signalling-a label of skin ageing? *PloS one* **7**, e50393 (2012).
18. Partridge, L. The new biology of ageing. *Philos. Transactions Royal Soc. B: Biol. Sci.* **365**, 147–154 (2010).
19. Kirkwood, T. B. Systems biology of ageing and longevity. *Philos. Transactions Royal Soc. B: Biol. Sci.* **366**, 64–70 (2011).
20. Mitsuyama, Y. *et al.* Chest radiography as a biomarker of ageing: artificial intelligence-based, multi-institutional model development and validation in japan. *The Lancet Heal. Longev.* **4**, e478–e486, DOI: [https://doi.org/10.1016/S2666-7568\(23\)00133-2](https://doi.org/10.1016/S2666-7568(23)00133-2) (2023).
21. Yashin, A. I., Stallard, E. & Land, K. C. *Biodemography of Aging: Determinants of Healthy Life Span and Longevity* (Springer, 2017).
22. Van der Laak, J., Litjens, G. & Ciompi, F. Deep learning in histopathology: the path to the clinic. *Nat. medicine* **27**, 775–784 (2021).
23. Litjens, G. *et al.* 1399 h&e-stained sentinel lymph node sections of breast cancer patients: the camelyon dataset. *GigaScience* **7**, giy065 (2018).
24. Wang, X. *et al.* Weakly supervised deep learning for whole slide lung cancer image analysis. *IEEE transactions on cybernetics* **50**, 3950–3962 (2019).
25. Syrykh, C. *et al.* Accurate diagnosis of lymphoma on whole-slide histopathology images using deep learning. *NPJ digital medicine* **3**, 63 (2020).
26. Tabibu, S., Vinod, P. & Jawahar, C. Pan-renal cell carcinoma classification and survival prediction from histopathology images using deep learning. *Sci. reports* **9**, 10509 (2019).
27. Rawat, R. R. *et al.* Deep learned tissue “fingerprints” classify breast cancers by er/pr/her2 status from h&e images. *Sci. reports* **10**, 7275 (2020).
28. Feng, Y., Zhang, L. & Mo, J. Deep manifold preserving autoencoder for classifying breast cancer histopathological images. *IEEE/ACM transactions on computational biology bioinformatics* **17**, 91–101 (2018).
29. Salle, F. G. *et al.* Comprehensive molecular and pathologic evaluation of transitional mesothelioma assisted by deep learning approach: a multi-institutional study of the international mesothelioma panel from the mesopath reference center. *J. thoracic oncology* **15**, 1037–1053 (2020).
30. Iizuka, O. *et al.* Deep learning models for histopathological classification of gastric and colonic epithelial tumours. *Sci. reports* **10**, 1504 (2020).
31. Kiani, A. *et al.* Impact of a deep learning assistant on the histopathologic classification of liver cancer. *NPJ digital medicine* **3**, 23 (2020).

32. Yang, H., Kim, J.-Y., Kim, H. & Adhikari, S. P. Guided soft attention network for classification of breast cancer histopathology images. *IEEE transactions on medical imaging* **39**, 1306–1315 (2019).
33. Liu, Y. *et al.* Detecting cancer metastases on gigapixel pathology images. *arXiv preprint arXiv:1703.02442* (2017).
34. Wang, D., Khosla, A., Gargeya, R., Irshad, H. & Beck, A. H. Deep learning for identifying metastatic breast cancer. *arXiv preprint arXiv:1606.05718* (2016).
35. Abhisheka, B., Biswas, S. K. & Purkayastha, B. A comprehensive review on breast cancer detection, classification and segmentation using deep learning. *Arch. Comput. Methods Eng.* **30**, 5023–5052 (2023).
36. Ullah, N. *et al.* Tumordetnet: A unified deep learning model for brain tumor detection and classification. *Plos one* **18**, e0291200 (2023).
37. Fremond, S. *et al.* Interpretable deep learning model to predict the molecular classification of endometrial cancer from haematoxylin and eosin-stained whole-slide images: a combined analysis of the portec randomised trials and clinical cohorts. *The Lancet Digit. Heal.* **5**, e71–e82 (2023).
38. Graham, S. *et al.* Mild-net: Minimal information loss dilated network for gland instance segmentation in colon histology images. *Med. image analysis* **52**, 199–211 (2019).
39. Graham, S. *et al.* Hover-net: Simultaneous segmentation and classification of nuclei in multi-tissue histology images. *Med. image analysis* **58**, 101563 (2019).
40. Bueno, G., Fernandez-Carrobles, M. M., Gonzalez-Lopez, L. & Deniz, O. Glomerulosclerosis identification in whole slide images using semantic segmentation. *Comput. methods programs biomedicine* **184**, 105273 (2020).
41. de Bel, T. *et al.* Automatic segmentation of histopathological slides of renal tissue using deep learning. In *Medical Imaging 2018: Digital Pathology*, vol. 10581, 285–290 (SPIE, 2018).
42. Pinckaers, H. & Litjens, G. Neural ordinary differential equations for semantic segmentation of individual colon glands. *arXiv preprint arXiv:1910.10470* (2019).
43. Naylor, P., Laé, M., Reyat, F. & Walter, T. Segmentation of nuclei in histopathology images by deep regression of the distance map. *IEEE transactions on medical imaging* **38**, 448–459 (2018).
44. Long, F. Microscopy cell nuclei segmentation with enhanced u-net. *BMC bioinformatics* **21**, 1–12 (2020).
45. Ding, K. *et al.* A large-scale synthetic pathological dataset for deep learning-enabled segmentation of breast cancer. *Sci. Data* **10**, 231 (2023).
46. Song, A. H. *et al.* Artificial intelligence for digital and computational pathology. *Nat. Rev. Bioeng.* **1**, 930–949 (2023).
47. Graham, S. *et al.* One model is all you need: multi-task learning enables simultaneous histology image segmentation and classification. *Med. Image Analysis* **83**, 102685 (2023).
48. Deng, R. *et al.* Segment anything model (sam) for digital pathology: Assess zero-shot segmentation on whole slide imaging. *arXiv preprint arXiv:2304.04155* (2023).
49. Li, C. *et al.* Weakly supervised mitosis detection in breast histopathology images using concentric loss. *Med. image analysis* **53**, 165–178 (2019).
50. Mahmood, T., Arsalan, M., Owais, M., Lee, M. B. & Park, K. R. Artificial intelligence-based mitosis detection in breast cancer histopathology images using faster r-cnn and deep cnns. *J. clinical medicine* **9**, 749 (2020).
51. Hou, L. *et al.* Sparse autoencoder for unsupervised nucleus detection and representation in histopathology images. *Pattern recognition* **86**, 188–200 (2019).
52. Swiderska-Chadaj, Z. *et al.* Learning to detect lymphocytes in immunohistochemistry with deep learning. *Med. image analysis* **58**, 101547 (2019).
53. Le, H. *et al.* Utilizing automated breast cancer detection to identify spatial distributions of tumor-infiltrating lymphocytes in invasive breast cancer. *The Am. journal pathology* **190**, 1491–1504 (2020).
54. Veta, M. *et al.* Predicting breast tumor proliferation from whole-slide images: the tupac16 challenge. *Med. image analysis* **54**, 111–121 (2019).
55. Nagpal, K. *et al.* Development and validation of a deep learning algorithm for improving gleason scoring of prostate cancer. *NPJ digital medicine* **2**, 48 (2019).
56. Jansen, I. *et al.* Automated detection and grading of non-muscle-invasive urothelial cell carcinoma of the bladder. *The Am. journal pathology* **190**, 1483–1490 (2020).



57. Karimi, D. *et al.* Deep learning-based gleason grading of prostate cancer from histopathology images—role of multiscale decision aggregation and data augmentation. *IEEE journal biomedical health informatics* **24**, 1413–1426 (2019).
58. Banerji, S. & Mitra, S. Deep learning in histopathology: A review. *Wiley Interdiscip. Rev. Data Min. Knowl. Discov.* **12**, e1439 (2022).
59. Komura, D. & Ishikawa, S. Machine learning methods for histopathological image analysis. *Comput. structural biotechnology journal* **16**, 34–42 (2018).
60. Roy, K., Banik, D., Bhattacharjee, D. & Nasipuri, M. Patch-based system for classification of breast histology images using deep learning. *Comput. Med. Imaging Graph.* **71**, 90–103 (2019).
61. Pinckaers, H., Van Ginneken, B. & Litjens, G. Streaming convolutional neural networks for end-to-end learning with multi-megapixel images. *IEEE transactions on pattern analysis machine intelligence* **44**, 1581–1590 (2020).
62. Codella, N. C. *et al.* Skin lesion analysis toward melanoma detection: A challenge at the 2017 international symposium on biomedical imaging (isbi), hosted by the international skin imaging collaboration (isic). In *2018 IEEE 15th international symposium on biomedical imaging (ISBI 2018)*, 168–172 (IEEE, 2018).
63. Weinstein, J. N. *et al.* The cancer genome atlas pan-cancer analysis project. *Nat. genetics* **45**, 1113–1120 (2013).
64. Zhu, W., Fernandez-Granda, C. & Razavian, N. Interpretable prediction of lung squamous cell carcinoma recurrence with self-supervised learning. *arXiv preprint arXiv:2203.12204* (2022).
65. Chen, C. *et al.* Fast and scalable search of whole-slide images via self-supervised deep learning. *Nat. Biomed. Eng.* **6**, 1420–1434 (2022).
66. Kanwal, N. *et al.* Detection and localization of melanoma skin cancer in histopathological whole slide images. In *2023 31st European Signal Processing Conference (EUSIPCO)*, 975–979 (IEEE, 2023).
67. Le Gallec, A. *et al.* Using deep learning to predict abdominal age from liver and pancreas magnetic resonance images. *Nat. Commun.* **13**, 1979 (2022).
68. Qiu, W., Chen, H., Kaeberlein, M. & Lee, S.-I. Explainable biological age (enabl age): an artificial intelligence framework for interpretable biological age. *The Lancet Heal. Longev.* **4**, e711–e723 (2023).
69. Heckenbach, I. *et al.* Nuclear morphology is a deep learning biomarker of cellular senescence. *Nat. Aging* **2**, 742–755 (2022).
70. Hofmann, S. M. *et al.* Towards the interpretability of deep learning models for multi-modal neuroimaging: Finding structural changes of the ageing brain. *NeuroImage* **261**, 119504 (2022).
71. Gialluisi, A. *et al.* Exploring domains, clinical implications and environmental associations of a deep learning marker of biological ageing. *Eur. J. Epidemiol.* **37**, 35–48 (2022).
72. Dinsdale, N. K. *et al.* Learning patterns of the ageing brain in mri using deep convolutional networks. *NeuroImage* **224**, 117401 (2021).
73. Chen, T. & Guestrin, C. Xgboost: A scalable tree boosting system. In *Proceedings of the 22nd acm sigkdd international conference on knowledge discovery and data mining*, 785–794 (2016).
74. Cox, D. R. Regression models and life-tables. *J. Royal Stat. Soc. Ser. B (Methodological)* **34**, 187–202 (1972).
75. Hautekiet, P. *et al.* A healthy lifestyle is positively associated with mental health and well-being and core markers in ageing. *BMC medicine* **20**, 328 (2022).
76. Davies, N. Promoting healthy ageing: the importance of lifestyle. *Nurs. Standard (through 2013)* **25**, 43 (2011).
77. Haveman-Nies, A., De Groot, L. C. & Van Staveren, W. A. Dietary quality, lifestyle factors and healthy ageing in europe: the seneca study. *Age ageing* **32**, 427–434 (2003).
78. Costantino, S., Paneni, F. & Cosentino, F. Ageing, metabolism and cardiovascular disease. *The J. physiology* **594**, 2061–2073 (2016).
79. Isaev, N. K., Genrikhs, E. E., Oborina, M. V. & Stelmashook, E. V. Accelerated aging and aging process in the brain. *Rev. Neurosci.* **29**, 233–240 (2018).
80. Branchet, M., Boisnic, S., Frances, C. & Robert, A. Skin thickness changes in normal aging skin. *Gerontology* **36**, 28–35 (1990).
81. Hazzard, W. R. Atherogenesis: why women live longer than men. *Geriatr. (Basel, Switzerland)* **40**, 42–51 (1985).

82. Ginter, E. & Simko, V. Women live longer than men. *Bratislavske lekarske listy* **114**, 45–49 (2013).
83. Waldron, I. & Johnston, S. Why do women live longer than men? *J. human stress* **2**, 19–30 (1976).
84. Eskes, T. & Haanen, C. Why do women live longer than men? *Eur. J. Obstet. & Gynecol. Reproductive Biol.* **133**, 126–133 (2007).
85. Austad, S. N. Why women live longer than men: sex differences in longevity. *Gend. medicine* **3**, 79–92 (2006).
86. Zarulli, V. *et al.* Women live longer than men even during severe famines and epidemics. *Proc. Natl. Acad. Sci.* **115**, E832–E840 (2018).
87. Hägg, S. & Jylhävä, J. Sex differences in biological aging with a focus on human studies. *Elife* **10**, e63425 (2021).
88. Ryan, C. P. *et al.* Pregnancy is linked to faster epigenetic aging in young women. *Proc. Natl. Acad. Sci.* **121**, e2317290121 (2024).
89. Chen, X. & He, K. Exploring simple siamese representation learning. In *Proceedings of the IEEE/CVF conference on computer vision and pattern recognition*, 15750–15758 (2021).
90. Azam, A. S. *et al.* Digital pathology for reporting histopathology samples, including cancer screening samples—definitive evidence from a multisite study. *Histopathology* (2024).
91. Romero Lauro, G. *et al.* Digital pathology consultations—a new era in digital imaging, challenges and practical applications. *J. digital imaging* **26**, 668–677 (2013).

## Supplementary

### Data availability

The digitised skin biopsies and registry data from the National Patient Register and other administrative registers used for this manuscript are person sensitive and are not publicly available. The data is stored at Statistics Denmark. Researchers affiliated with a Danish research institution can gain access to all non-image data via [Statistics Denmark's Research Services](#). Access to the digitized skin biopsies requires an ethical approval from the Danish Research Ethics Committees. The code for the preprocessing step of contrastive deep learning, as well as the downstream tasks, has been made available at this [Github repository](#). For further information, contact the authors.